



**HAL**  
open science

# A tomographic crustal velocity model of the central Fennoscandian Shield

T. Hyvonen, T. Tiira, A. Korja, P. Heikkinen, E. Rautioaho

► **To cite this version:**

T. Hyvonen, T. Tiira, A. Korja, P. Heikkinen, E. Rautioaho. A tomographic crustal velocity model of the central Fennoscandian Shield. *Geophysical Journal International*, 2007, 168 (3), pp.1210 à 1226. 10.1111/j.1365-246X.2006.03242.x . insu-00346260

**HAL Id: insu-00346260**

**<https://insu.hal.science/insu-00346260>**

Submitted on 5 Mar 2021

**HAL** is a multi-disciplinary open access archive for the deposit and dissemination of scientific research documents, whether they are published or not. The documents may come from teaching and research institutions in France or abroad, or from public or private research centers.

L'archive ouverte pluridisciplinaire **HAL**, est destinée au dépôt et à la diffusion de documents scientifiques de niveau recherche, publiés ou non, émanant des établissements d'enseignement et de recherche français ou étrangers, des laboratoires publics ou privés.

# A tomographic crustal velocity model of the central Fennoscandian Shield

Tellervo Hyvönen, Timo Tiira, Annakaisa Korja, Pekka Heikkinen, Elisa Rautioaho and the SVEKALAPKO Seismic Tomography Working Group

*Institute of Seismology, FI-00014 University of Helsinki, Helsinki, Finland. E-mail: Tellervo.Hyvonen@helsinki.fi*

Accepted 2006 September 28. Received 2006 September 5; in original form 2005 May 23

## SUMMARY

In this paper, local seismic tomographic method is used to find the terrane distribution within the central parts of the accretionary Svecofennian Orogen. This study presents a crustal  $P$ -wave velocity model, and for the first time the  $S$ -wave velocity and  $V_p/V_s$  ratio model of SVEKALAPKO area that is  $700 \times 800 \text{ km}^2$  in southern and central Finland. The 3-D model is presented as  $P$ - and  $S$ -wave velocity as well as  $V_p/V_s$  ratio depth slices and vertical sections.

The data set comprised of several subsets of crustal  $Pg$ - and  $Sg$ -wave traveltime data: from local events recorded by the SVEKALAPKO seismic tomography array in 1998–1999, from older controlled source shots recorded at portable stations as well as at permanent stations, and from non-controlled chemical explosions recorded at permanent seismic stations. From 300 local explosions a total of 10 404  $Pg$ -wave and 9361  $Sg$ -wave arrival times were inverted to create independent 3-D  $V_p$  and  $V_s$  tomographic models, from which the  $V_p/V_s$  ratio was calculated. According to sensitivity tests, the optimal horizontal resolution of recognizable velocity structures in the central study area is at least 60 km down to depths of 40 km.

In the final model, the seismic velocities vary smoothly. The lateral variations are larger for  $V_p$  ( $5.9\text{--}6.6 \text{ km s}^{-1}$ ) than for  $V_s$  ( $3.5\text{--}3.8 \text{ km s}^{-1}$ ) in the upper 20 km of the crust. At depths of 20–40 km,  $V_p$  varies from 6.5 to  $7.2 \text{ km s}^{-1}$  and  $V_s$  from 3.7 to  $4.1 \text{ km s}^{-1}$ . The  $V_p/V_s$  ratio varies spatially more distinct than  $P$ - and  $S$ -wave velocities, usually from 1.70 to 1.74 in the upper crust and from 1.72 to 1.78 in the lower crust. Schist belts and their continuations at depth are associated with lower velocities and lower  $V_p/V_s$  ratios ( $V_p < 6.2\text{--}6.8 \text{ km s}^{-1}$ ;  $V_s < 3.6\text{--}3.9 \text{ km s}^{-1}$ ;  $V_p/V_s = 1.68\text{--}1.73$ ) than the granitoid areas ( $V_p = 6.3\text{--}7.4 \text{ km s}^{-1}$ ;  $V_s = 3.6\text{--}4.2 \text{ km s}^{-1}$ ;  $V_p/V_s = 1.72\text{--}1.78$ ).

The Svecofennian Orogen was accreted from crustal blocks ranging in size from  $100 \times 100 \text{ km}^2$  to  $200 \times 200 \text{ km}^2$  in cross-sectional area. The intervening sedimentary belts have *ca.*  $0.2 \text{ km s}^{-1}$  lower  $P$ - and  $S$ -wave velocities and *ca.* 0.04 lower  $V_p/V_s$  ratios. Tomographic model supports the idea that the thick Svecofennian crust was accreted from several crustal terranes, some hidden, and that the crust was later modified by intra and underplating.

**Key words:** crust, Fennoscandia, Finland,  $P$  wave, Precambrian,  $S$  wave, seismic velocity,  $V_p/V_s$  ratio.

## INTRODUCTION

The SVEKALAPKO seismic tomographic network (Bock *et al.* 2001; Hjelt *et al.* 1996) in the Fennoscandian Shield was launched to study the structure of the stable continental lithosphere (Fig. 1). Continental crust began to form already in the Archean but the stable cratonic shields were only formed in the Palaeoproterozoic. Lately many studies have focused on the formation mechanisms of the shields, as they are the cores of the modern continents. Global crustal compilations (Mooney *et al.* 1998; Bassin *et al.* 2000) suggest that the Precambrian crust is thicker than

the modern continental crust. This indicates modification in either the processes or the physical/chemical properties of the crust.

The seismic activity is low in Finland. During the last 20 yr on the average 10–15 earthquakes occurred annually, majority of events had magnitude smaller than 3.0, and the largest event felt in Finland was  $M_L = 3.8$  earthquake in 1979. The bedrock in Finland is Precambrian: Archean in the northeast and Palaeoproterozoic in the southwest (Fig. 1). The boundary zone between the Archean and Proterozoic is complex, highly fractured and oriented in NW–SE direction.

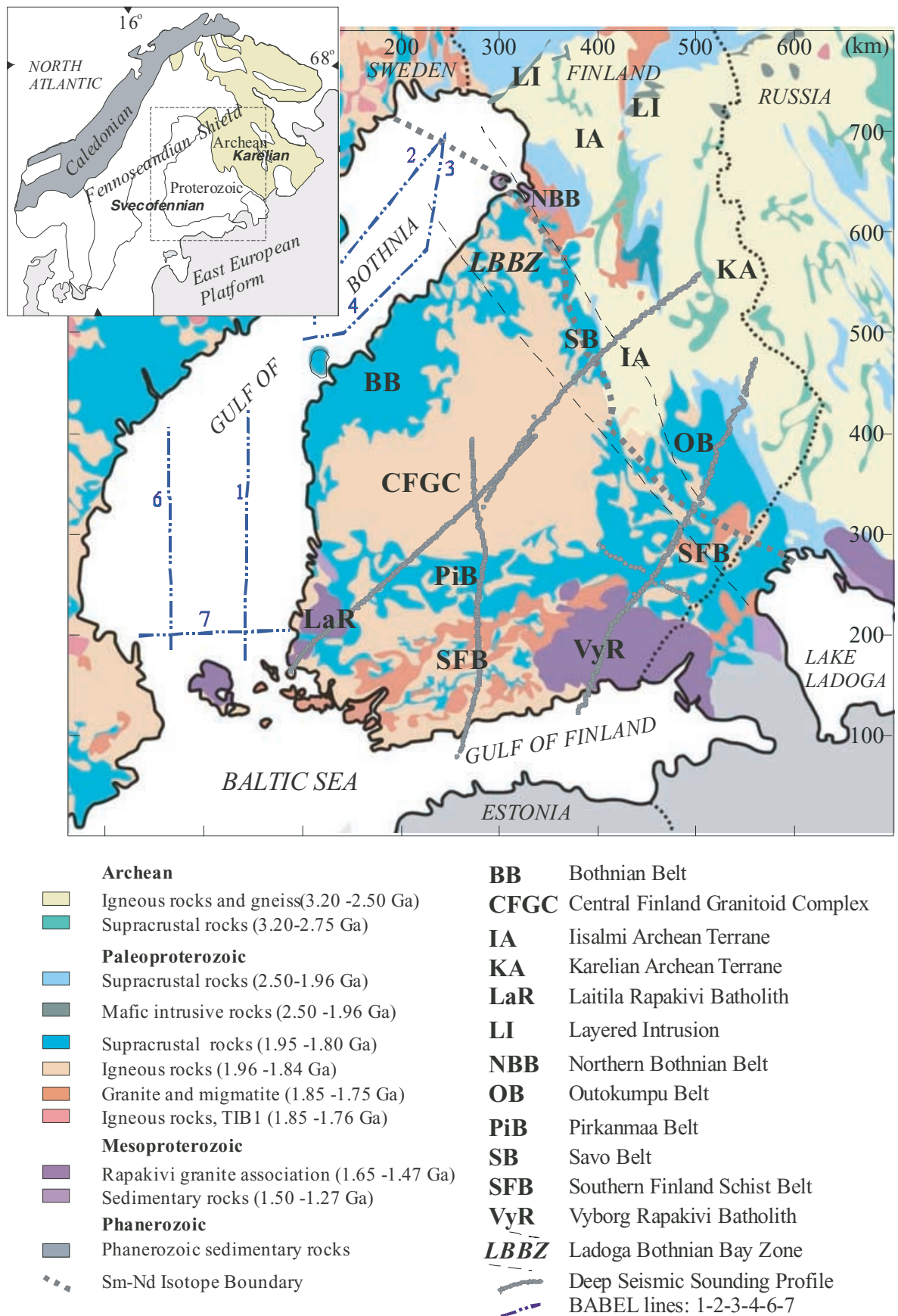


Figure 1. General lithological map of the study area in southern and central Finland after Koistinen *et al.* (2001).

Previous refraction and reflection studies reveal an abnormally thick crust (>56 km) with large crustal thickness variations (42–65 km; Luosto 1997; Korsman *et al.* 1999). The largest crustal depression is observed along the Archean-Proterozoic suture zone and the largest upwarping beneath the Mesoproterozoic rapakivi granitoids. Although the refraction studies describe the crust as a three-layer model: upper, middle and lower crust (Luosto 1991; Luosto *et al.* 1990, 1995; Luosto 1997), reflection studies (BABEL Working Group 1993; Korja & Heikkinen 2005) point out major structural discontinuities and a highly complex 3-D structure. Reflection studies suggest that the size of velocity anomaly is *ca.* 100–150 km in lateral dimensions (Korja & Heikkinen 2005). Similar size heterogeneities have also been detected in  $V_p/V_s$  models of the refraction studies (Luosto *et al.* 1989).

Based on crustal thickness variations and other geophysical and geological data Korja *et al.* (1993) and Lahtinen *et al.* (2005) have suggested that the Palaeoproterozoic part of the Fennoscandian Shield is composed of island arcs, microcontinental fragments and intervening sedimentary basins. In modern island arc environments sedimentary basins (accretion prism, forearc basin, backarc basin) have lower seismic velocities than the arcs and continents (Suyehiro *et al.* 1996; Van Avendonk *et al.* 2004; Clowes *et al.* 2005). It is assumed that this relationship holds even after collision and that different tectonic units can be identified based on their seismic velocity distributions.

To study the real spatial distribution of the proposed arcs, continental fragments and sedimentary basins a rather detailed 3-D velocity model is required. Additional control on the structural variations

can be deduced from  $S$ -wave velocity and  $V_p/V_s$  ratio distributions. The  $V_p/V_s$  ratio distribution is especially interesting as it is independent of density and determines uniquely the Poisson's ratio—a measure of incompressibility of material. The  $V_p/V_s$  ratio carries information on elastic properties of bedrock and thus on its composition and deformational history.

Previously few attempts have been made to study the 3-D seismic structure of the crust in Finland. From the rather dense network of refraction lines (line spacing 200–300 km), first Luosto (1991, 1997) and then Kinck *et al.* (1993) and Korsman *et al.* (1997) interpolated the depth to the Moho-map of the area. These were soon followed by maps of the thickness of the lower crust and upper–middle crust (Korja *et al.* 1993). The same data sets were recently used by Sandoval *et al.* (2003) who compiled a smoothed 3-D reference  $P$ -wave velocity model for SVEKALAPKO mantle tomography studies (Bruneton *et al.* 2002, 2004a,b; Alinaghi *et al.* 2003; Friederich *et al.* 2004; Sandoval *et al.* 2004) by weighting the previous controlled source results. Based on data from local explosions detected by the SVEKALAPKO array Kozlovskaya *et al.* (2004) modified the crustal reference model and inverted a 3-D density model for the crust. Few other inversion studies were conducted in the central part of the shield. Luosto *et al.* (1990) presented a 2-D generalized inversion for  $P$ - and  $S$ -wave velocities in the upper crust along the BALTIC profile (Fig. 2a), and Hole *et al.* (1996) studied the BABEL profiles 1 and 6 (Fig. 1). Burmakov *et al.* (1991) and Poupinet *et al.* (1993) used a  $P$ -wave tomography along the BALTIC and the SVEKA-81 (Grad & Luosto 1987) profiles, respectively. Malaska & Hyvönen (2000) created the first local 3-D

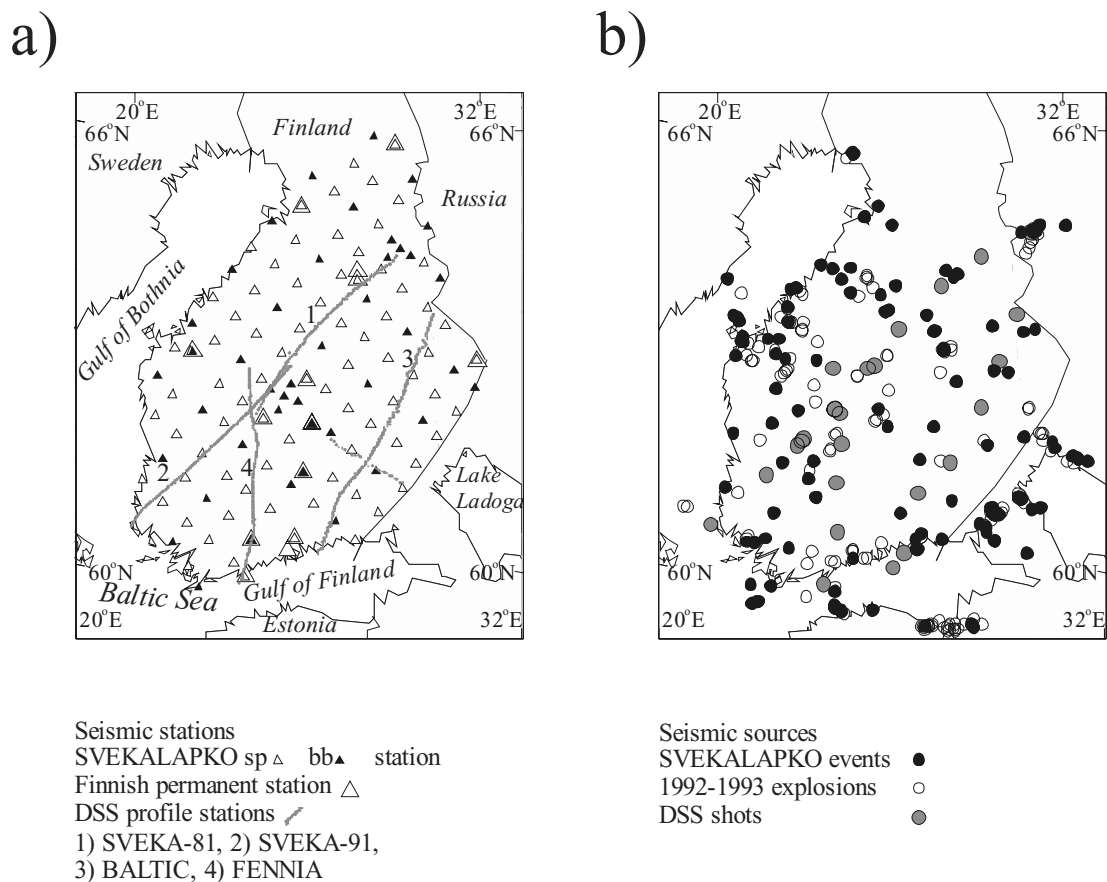


**Figure 2.** Seismic stations (a) and sources (b) used in this study. The maps are plotted using the Generic Mapping Tool—routines (Wessel & Smith 1998).

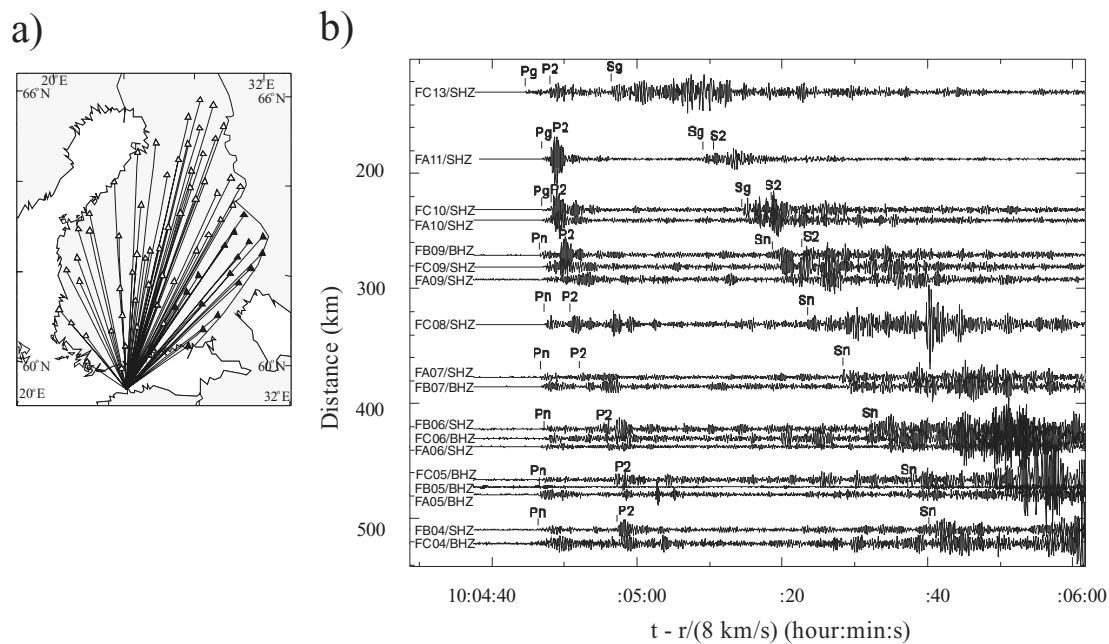


**Figure 3.** An example of a good quality event recorded by SVEKALAPKO array: (a) The  $M_L$  2.9 explosion offshore Estonia was recorded by 77 SVEKALAPKO stations on November 5th, 1998. Black triangles mark the stations from where the seismograms are shown. (b) The seismograms (3–6 Hz bandpass filtered) are presented in azimuth sector of  $30^\circ$ – $60^\circ$  from the epicentre. Crustal ( $P_g$ ,  $S_g$ ) and mantle ( $P_n$ ,  $S_n$ )-wave arrivals and some distinct reflections ( $P_2$ ,  $S_2$ ) are marked above the recordings.

crustal  $P$ -wave model by using both permanent and portable station observations of the controlled source experiments.

During the EUROPROBE/SVEKALAPKO seismic tomography experiment (Raita 2001; Bock *et al.* 2001), a network of 143 stations in  $50 \text{ km} \times 50 \text{ km}$  grid was installed over southern and central Finland, extending to NW Russia. The full seismic array operated for 6 months from 1998 October 1998 to 1999 March and produced good quality recordings of weak local events distributed over southern and central Finland.

In this paper, we use 132 well-recorded local events from the SVEKALAPKO array data set together with other previously published data sets (Figs 2 and 3) to calculate a 3-D absolute  $P$ -wave velocity model. We also present the first absolute  $S$ -wave velocity and  $V_p/V_s$  ratio models for the crust. Because the  $S$  wave velocity model is inverted independently of the  $P$ -wave velocity model, a real  $V_p/V_s$  ratio model is derived. The model will be correlated with the surface geology, and with the previously suggested crustal block geometry. The geological implications of the model will be discussed.

## TOMOGRAPHY PROCEDURE

The 3-D tomographic inversion was computed using the program Jive3D (Hobro 1999; Hobro *et al.* 2003). The program is based on the 2-D inversion algorithm of McCaughey & Singh (1997). The Jive3D tomography program produces velocity models using layer-interface formalism, and traveltimes of direct, refracted, and reflected seismic waves. Only refracted crustal turning waves were used in this study. The non-linear problem is approximated as a series of linear steps. An iterative inversion approach regularized least-square solution and conjugate gradient method for optimization (e.g. Press *et al.* 1992) are used. A linearized, regularized model space is inverted by optimizing the model fit with traveltime data to result in a smooth minimum structure velocity model. Variable

smoothing method is adopted from Williamsson (1990), and the forward problem is solved by ray tracing method of Farra (1990).

The tomography process was started by defining the initial velocity model and solving the forward problem. Optimal iteration path giving the minimum data misfit, where the convergence stopped, was defined, and the ‘near-final’ model was computed. Using the ‘near-final’ model the non-controlled source events were relocated by grid search technique. Inversion of the relocated data produced the final tomography  $P$ - and  $S$ -wave velocity and  $V_p/V_s$  models.

## Data

In this study traveltimes of crustal turning rays,  $P_g$  and  $S_g$ , from local mining explosions, quarry blasts and controlled source shots were inverted (local magnitude  $M_L < 3$ ; Fig. 2b). The study region was located between longitudes  $20^\circ$ – $32^\circ$ E and latitudes  $59^\circ$ N– $66^\circ$ N covering southern and central Finland. The ( $x$ ,  $y$ ,  $z$ ) origin was set at  $59^\circ$ N,  $20^\circ$ E at the sea level. The topography of the ground surface was included in the model. For the zero-depth explosions, seismic rays were traced to start and finish at the ground surface. For successful rays reaching the target receivers, the maximum source–receiver distance was 296 km; thus, the use of the Cartesian coordinate system (Ollikainen & Ollikainen 2004) and flat earth assumption was justified.

## SVEKALAPKO data

The 1998–1999 SVEKALAPKO seismic tomography network (Fig. 2a) had a station spacing of 50 km. The aim was to get as evenly spread and dense epicentre distribution as possible inside the study area (Figs 2b and 3). For this study, 132 well-recorded events with distinct  $P$ - and  $S$ -wave onsets were selected. The number of stations with good quality recording per event varied from seven

to 111. Before picking arrival times, the seismograms of an event were sorted according to increasing epicentre distance, and organized into 30° azimuth sectors around the epicentre. If the sector included less than 10 seismograms, the sector size was increased (sometimes up to 360°). Each sector was analysed separately, allowing phase correlation between neighbouring stations and the estimation of the crossover distance, at which the crustal waves,  $P_g$  and  $S_g$ , transform to the mantle refracted waves,  $P_n$  and  $S_n$ , respectively. The large seismogram separation (i.e. the distance between neighbouring stations; > 10 km) resulted sometimes in poorly identified crossover distance. For this reason, at distance range of 200–300 km the data set included some  $P_n$  and  $S_n$  phases, which could result in increased lower crustal velocities. In order to abolish these phases the Moho boundary of Sandoval *et al.* (2003) was included in the *a priori* model. However, some mantle phases still may have been incorporated in the data due to the uncertainties in the Moho depth map. For the same reason some crustal phases might have been traced as mantle phases and missed from inversions.

An example of a good quality SVEKALAPKO recording is given in Fig. 3; the seismograms of the  $M_L$  2.9 explosion offshore Estonia are plotted with increasing distance in an azimuth sector of 30°–60°. In this sector, the seismogram separation varies from 10 to 50 km. This is typical for events that have good station coverage. The  $P$ -wave arrivals were picked from unfiltered or from 2 to 8 Hz bandpass filtered recordings. The 3–6 Hz bandpass filtering was applied when picking  $S$ -wave arrivals.

#### Controlled source data

In southern and central Finland during past two decades, several deep seismic sounding (DSS) profiles were surveyed. The DSS lines were oriented in N–S and NE–SW direction extending to lengths of 300–500 km and sampled the crust and upper mantle to depths of 70–100 km. The  $P_g$ - and  $S_g$ -wave traveltimes from the 26 shots along four DSS lines: SVEKA-81 (Grad & Luosto 1987; Luosto 1991), BALTIC (Luosto *et al.* 1990), SVEKA-91 (Luosto *et al.* 1995) and FENNIA (Heikkinen *et al.* 1998) (Fig. 2a) were included in the tomography input data, referred as the ‘DSS on-line data’. The DSS on-line data was picked using program ZPLOT (Zelt 1994; Šroda 1999). The change from crustal to mantle waves was possible to identify for the DSS data because the station spacing was 2 km.

#### Permanent station data

In addition, two older data sets (Hyvönen & Sanina 1996; Malaska & Hyvönen 2000) recorded by the Finnish permanent station network were included in this study. The first data set consists of  $P_g$ - and  $S_g$ -wave arrivals from 142 local events with magnitude  $M_L \geq 2$  occurring between 1992 October–November and 1993 January–March. The second data set, referred here as the ‘DSS off-line data’, consists of  $P_g$  and  $S_g$  arrivals from 26 DSS shots. The arrival times of seismic signals at the permanent and SVEKALAPKO stations, were handpicked using an interactive data analysis and display program Geotool (Henson & Coyne 1995). The picking involved a large amount of events and stations, and several filtering and zooming steps were needed to detect the very first absolute onset, and to identify the correct phase. The accuracy of an individual pick depended on the magnitude of the event, on the epicentral distance and on the quality of the recording. If the seismogram had a low signal-to-noise ratio, the pick was discarded.

## Tomographic inversion

The tomography process was started by defining the initial velocity model, a horizontally homogeneous velocity distribution with a vertical velocity gradient. The velocity field was parametrized as a regular grid of evenly spaced velocity nodes and the velocities were interpolated by quadratic  $B$  splines. From each source a fan of rays was shot and each fan consisted of rays with 30 evenly spaced ray directions inside a sector with take-off angle of 40°–90° (0° indicates downward direction) and azimuthally 60 evenly spaced ray directions with 360° coverage. Using results from fan shooting, the ray tracing was continued for each receiver until rays reached receiver positions with  $\pm 0.04$  km accuracy.

#### Influence of the *a priori* model

The Jive3D program is rather independent of the initial model (Hobro 1999). This was tested with five different *a priori* models by varying vertical velocity gradients in horizontally homogeneous model space (Fig. 4a). The data set was inverted using same inversion parameters as the final inversion with the five different starting models. The inversion results were compared by calculating maximum velocity differences between the resulting models in 1-D velocity-depth functions at 30 evenly placed points inside the central study area ( $x = 150$ – $400$  km,  $y = 200$ – $400$  km,  $\delta x = \delta y = 50$  km;  $z = 0$ – $40$  km,  $\delta z = 0.05$  km). As a result, 90 per cent of the maximum  $P$ -wave velocity differences (of 24 030 values) were less than  $0.04$  km s<sup>-1</sup> (Fig. 4b). Average of all maximum differences was  $0.023$  km s<sup>-1</sup>. The largest differences were observed in areas of poor resolution.

#### Data uncertainty

In the inversion 10 404  $P$ -wave arrival times and 9361  $S$ -wave arrival times of seismic waves propagating in the crust were used. In the inversion, the traveltimes were given uncertainty values according to estimated picking accuracy. For the DSS on-line data the uncertainty ( $W$ ) for  $P$ -wave arrivals was  $W_p = 0.05$  s, and for  $S$ -wave arrivals  $W_s = 0.15$  s, for the DSS off-line data:  $W_p = 0.2$  s,  $W_s = 0.4$  s, and for the SVEKALAPKO and the non-controlled source data:  $W_p = 0.3$  s,  $W_s = 0.5$  s. During the first inversions, the traveltimes with large absolute residuals (> 2 s, about 2 per cent of data) were gradually removed because they were considered erroneous and not correlated with the structure. In the final model, the average residual was 0.20 s for  $P$  picks and 0.36 s for  $S$  picks. The average residuals and the number of picks for different data sets are presented in Table 1.

#### Convergence of the solution

During the inversion process, the data misfit decreased and the roughness of the model increased as the model converged, producing more details in the structure. The convergence was controlled by stepwise decrease in regularization strength and in percentage of full optimization for conjugate gradient algorithm, and a smooth minimum structure model was obtained. At the start of new iteration, rays were traced in the model from the previous iteration, and initial error estimates were computed for this iteration. The model was updated and final error estimates were computed for this iteration. The convergence of the solution was monitored by the following estimators: number of successfully traced rays, model

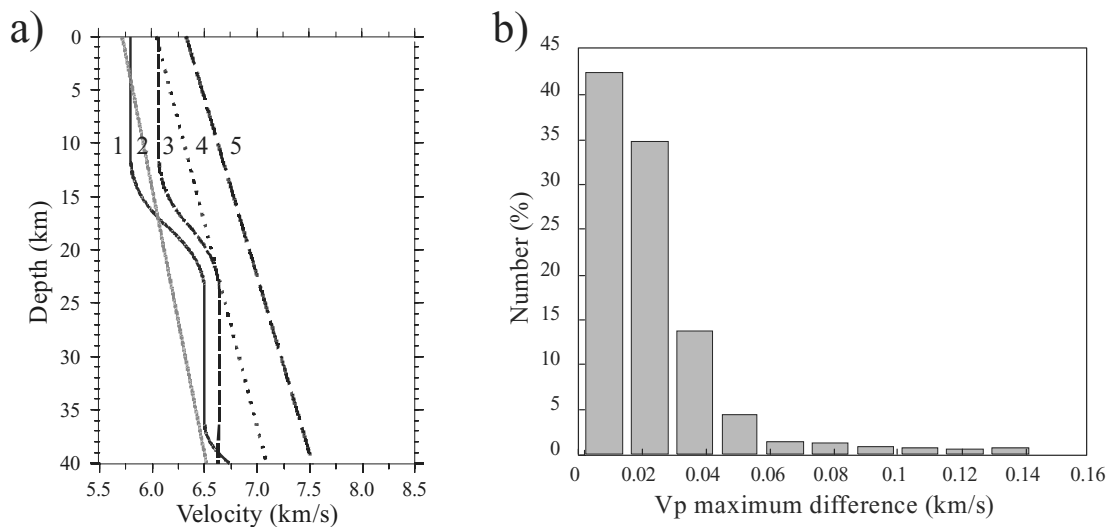


**Figure 4.** Testing *a priori* models. (a) Velocity-depth curves of five different *a priori* models: (1) IASPEI; (2) low velocity gradient; (3) model in Table 2; (4) model used in this study and (5) high velocity gradient. (b) Maximum differences ( $\text{km s}^{-1}$ ) in the velocity fields of the final inverted models are shown.

**Table 1.** Number of arrival times and absolute mean residuals for different data sets.

Data set	Number of <i>P</i> wave Arrivals (*)	Absolute mean <i>Pg</i> Wave residual (s)	Number of <i>S</i> wave Arrivals (*)	Absolute mean <i>Sg</i> Wave residual (s)
DSS On-line	2973	0.047	1831	0.132
DSS Off-line	264	0.253	275	0.421
SVEKALAPKO	6077	0.302	6132	0.463
1992–1993 events	1090	0.261	1123	0.408
All	10 404	0.202	9361	0.364

(\*) *P*- and *S*-wave arrivals include some mantle phases not used in the inversions.

roughness, data misfit, and  $\chi^2$  values. The inversion process was interrupted when the following criteria were fulfilled simultaneously: the number of successful rays started to decrease, the initial data misfit and the final data misfit parameters, and the initial  $\chi^2$  values and final  $\chi^2$  values started to diverge. For the DSS on-line data, 95 per cent of *Pg* rays and 98 per cent of *Sg* rays were successfully traced. The corresponding percentages cannot be defined for the non-controlled source data due to the presence of the mantle *Pn* and *Sn* phases. The error estimates for the final model were  $\chi^2 = 1.8$  for the *P*-wave velocity model and  $\chi^2 = 1.5$  for the *S*-wave velocity model. The  $\chi^2$  values were larger for the *P* waves than for the *S* waves. This could be caused by overestimation of the *S*-wave data uncertainties or by underestimation of the *P*-wave data uncertainties.

## Relocation

The data set was dominated by non-controlled events (91 per cent). The non-controlled source events were located using a 1-D mean velocity model with a 50 km thick crust (Table 2). These locations

**Table 2.** 1-D crustal velocity model used in location of non-controlled sources.

Layer (km)	<i>P</i> -wave velocity ( $\text{km s}^{-1}$ )	<i>S</i> -wave velocity ( $\text{km s}^{-1}$ )
0–19	6.07	3.51
19–50	6.64	3.84
50–90	8.03	4.64
>90	8.50	4.75

were considered as preliminary locations for the 1992–1993 events and for the SVEKALAPKO events. The location accuracy was better for the SVEKALAPKO events owing to the denser receiver network. The epicentre locations were biased due to the discrepancy between the 3-D crustal structure and the simplified 1-D velocity model. Some bias arises also from the large azimuth gap for events close to the study area margins.

The data was inverted and the best-fit 3-D velocity structure was obtained. With this ‘near-final’ velocity model, the non-controlled sources were relocated by a grid search method with a regular grid of 121 trial locations around the original hypocentre with zero focal depth. The new location was set according to the minimum mean residual, new *P*- and *S*-wave velocity models were inverted, and updated traveltimes were calculated. A stepwise search was carried out with a grid spacing of 2, 1 and 0.5 km, each step starting with best previous location as the grid centre. The *P* picks were weighted by 1.0 and the *S* picks by 0.5 in the relocation. If the number of successfully traced rays dropped below five, the event was not relocated. If the number of rays used for location were small, the grid search algorithm would converge to a local minimum instead of global minimum, if some of the picks were not accurate. In the relocation process the average residual of all events dropped from 0.32 to 0.20 s for *P* waves and from 0.52 to 0.36 s for *S* waves, respectively.

The average location correction was  $\pm 2.4$  km for the SVEKALAPKO events and  $\pm 3.4$  km for the other non-controlled events. The relocation of the controlled source DSS shots with known locations, using data only from the permanent stations, resulted in an average location error of  $\pm 1.6$  km. This was estimated to be an error for the other events recorded only by the permanent

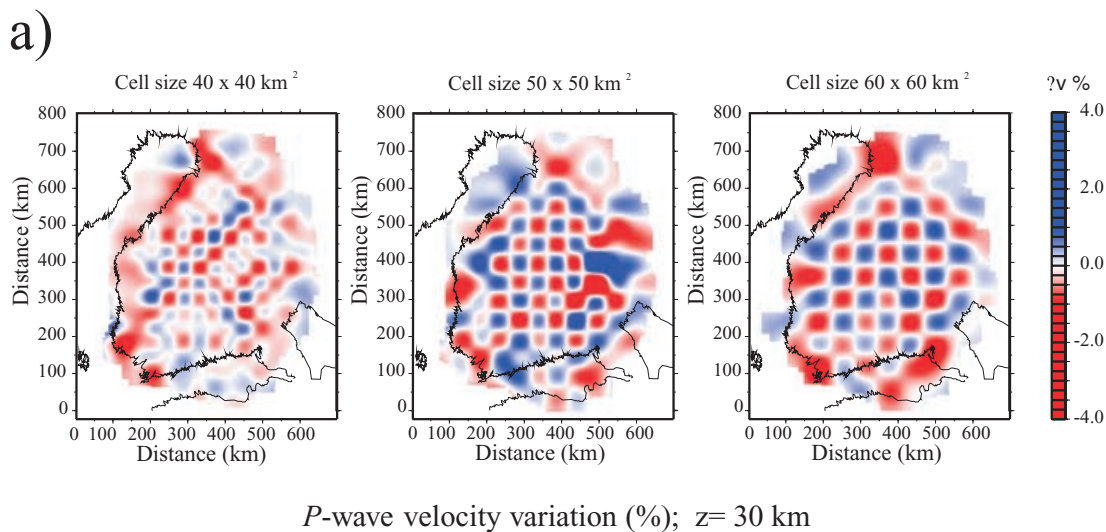


**Figure 5.** Lateral resolution according to checkerboard tests. (a)  $P$ -wave velocity resolution at depth of 30 km for different horizontal cell sizes. (b)  $P$ - and  $S$ -wave velocity resolution at depths of 10 and 40 km in cell size of  $60 \times 60 \text{ km}^2$ . Black line outlines the region with good resolution where checkerboard pattern is visible.

stations. After relocation, the final velocity structure was solved.

### Resolution

Checkerboard testing by the available data is a common method (e.g. Zelt 1998; Tong 2002). Spatial resolution for  $P$ -wave velocity is tested here using checkerboard cell sizes of  $40 \times 40 \times 4$ ,  $50 \times 50 \times 5$ , and  $60 \times 60 \times 6 \text{ km}^3$ . The velocity model is perturbed by alternating the velocities in adjacent cells by  $\pm 4$  per cent. The resolution test results for  $P$ -wave velocity at depth of 30 km are shown in Fig. 5(a). The recovered horizontal pattern was best resolved for the model cell size of  $60 \times 60 \text{ km}^2$ . The recovered checkerboard pattern is visualized for  $P$ - and  $S$ -wave velocities at depths of 10 and 40 km in Fig. 5(b).

The velocity structure was resolved horizontally to at least size of  $60 \times 60 \text{ km}^2$  in the inverted models, especially in the central area and close to the DSS lines (Figs 2a, 5 and 6). The data consisted mainly of  $P_g$  and  $S_g$  arrivals, and number of rays travelling in the lowermost crust was small resulting poor resolution in the lower crust. Therefore, the results were limited to the upper and middle crust to depth of 40 km.

To eliminate the effect of the position of the velocity grid to the final model, the grid model was displaced to nine different positions by moving the grid by half of the grid size (30 km). For each grid, the velocity structure was inverted, and an average model of nine was calculated. This technique smoothed away smaller details from the model.

## RESULTS

The  $V_p$ ,  $V_s$  and  $V_p/V_s$  distributions are presented on horizontal slices in Fig. 6 and on vertical cross-sections along four E–W and N–S oriented profiles in Fig. 7. The final models expressed smooth variations in both  $V_p$  and  $V_s$  distributions. The velocity variations at depths of 10 and 20 km were *ca.*  $\pm 0.1 \text{ km s}^{-1}$  from the average for  $P$  waves (Fig. 6a), *ca.*  $\pm 0.05 \text{ km s}^{-1}$  for  $S$  waves (Fig. 6b), and *ca.*  $\pm 0.03$  for  $V_p/V_s$  ratio. At depths of 20 and 40 km, the veloc-

ity variations were *ca.*  $\pm 0.2 \text{ km s}^{-1}$  from the average for  $P$  waves (Fig. 6a), *ca.*  $\pm 0.1 \text{ km s}^{-1}$  for  $S$  waves (Fig. 6b), and *ca.*  $\pm 0.06$  for  $V_p/V_s$  ratio (Fig. 6c). Although the variations were in general smooth, the local  $P$ -wave velocity could change laterally up to  $0.4 \text{ km s}^{-1}$  at distance of 100 km (e.g. from  $6.8$  to  $7.2 \text{ km s}^{-1}$  in Fig. 6a,  $z = 30 \text{ km}$ ) imposing a large horizontal gradient better displayed in  $V_p/V_s$  ratio maps (Fig. 6c).

On the velocity maps (Figs 6 and 7), the  $V_p$  anomalies are laterally *ca.* 100 km and  $V_s$  anomalies *ca.* 200 km in size in the upper and middle crust. A slightly larger anomaly in the lower crust might be a direct consequence of sparsely distributed rays and of lack of deep sources, or it could reflect larger crustal block size at depth. Although the  $V_p/V_s$  ratios between 1.68 and 1.80 were found throughout the upper 40 km of the crust (Fig. 6c), the average value increased with depth as previously observed by Luosto *et al.* (1990). The volume of rock with values  $< 1.72$  was greater in the uppermost 20 km. The  $V_p/V_s$  ratio anomalies showed pronounced horizontal gradients, and their local minima and maxima were more distinct than the  $V_p$  and  $V_s$  ones. The size of the  $V_p/V_s$  ratio anomalies varied between  $100 \times 100$  and  $200 \times 200 \text{ km}^2$ . Overall, the schist belts (Bothnian Belt, Pirkanmaa Belt and Savo Belt) and their continuations at depth were associated with lower velocities and  $V_p/V_s$  ratios ( $V_p < 6.2\text{--}6.8 \text{ km s}^{-1}$ ;  $V_s < 3.6\text{--}3.9 \text{ km s}^{-1}$ ;  $V_p/V_s = 1.68\text{--}1.73$ ) than the granitoid areas. For the granitoid areas (Karelian Archean terrane, Central Finland Granitoid Complex, Laitila Rapakivi granite and Vyborg Rapakivi granite) the velocity range was also larger ( $V_p = 6.3\text{--}7.4 \text{ km s}^{-1}$ ;  $V_s = 3.6\text{--}4.2 \text{ km s}^{-1}$ ;  $V_p/V_s = 1.72\text{--}1.78$ ).

Overall, in vertical sections (Fig. 7) the  $V_s$  variations are smoother than  $V_p$  or less perturbed. The E–W oriented vertical cross-sections (Fig. 7a) indicate a slight increase of both  $V_p$  and  $V_s$  from west to east, suggesting that the Archean crust is characterized by slightly higher average of the seismic velocity than the Proterozoic crust. This effect is enhanced by the low velocities associated with the Bothnian Belt located at the western end of the sections. The N–S oriented vertical cross-sections (Fig. 7b) show a slight increase of velocities towards the south, indicating that the southern Finland complex consists of higher velocities than the Central Finland complex.

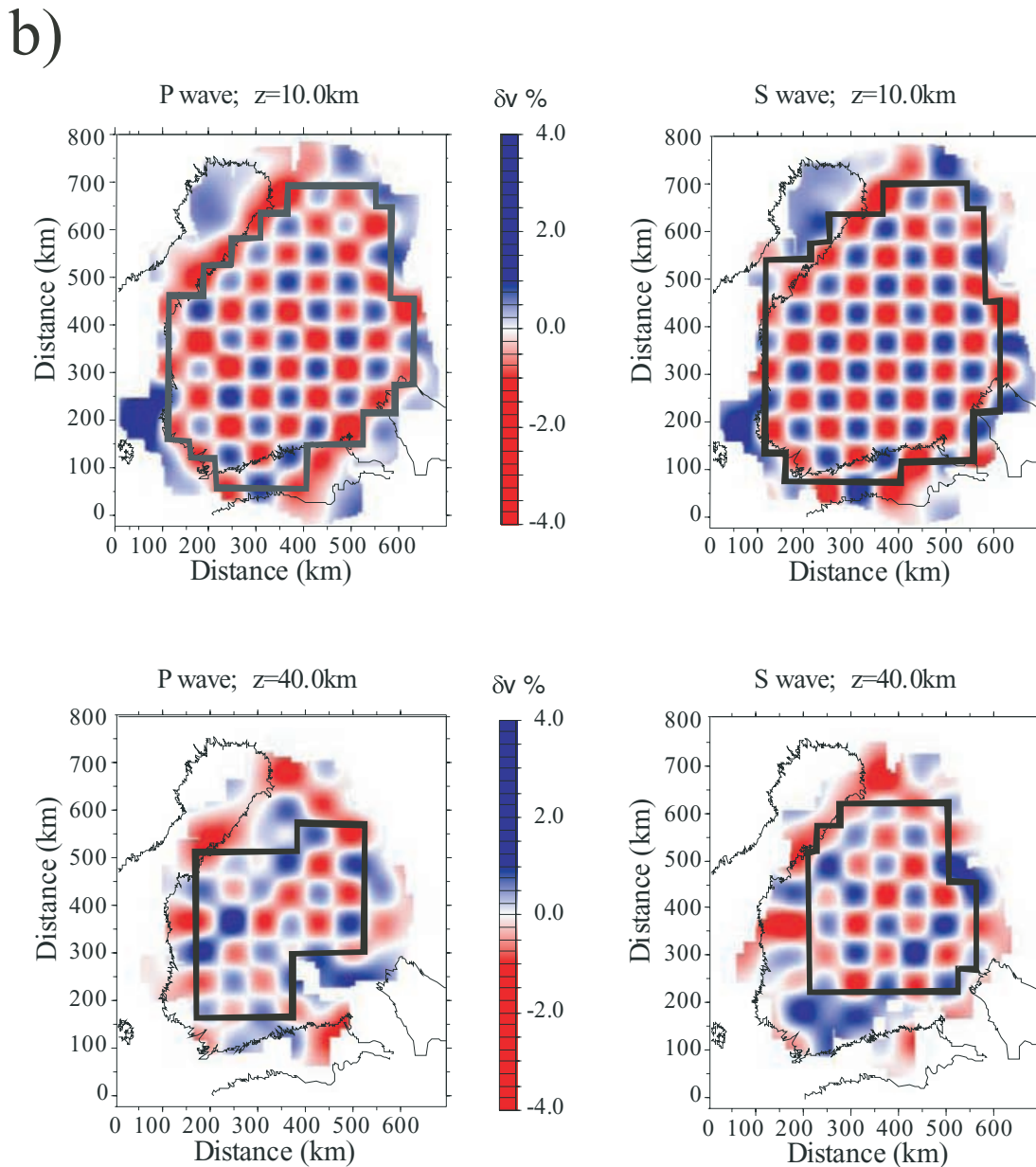


Figure 5. (Continued.)

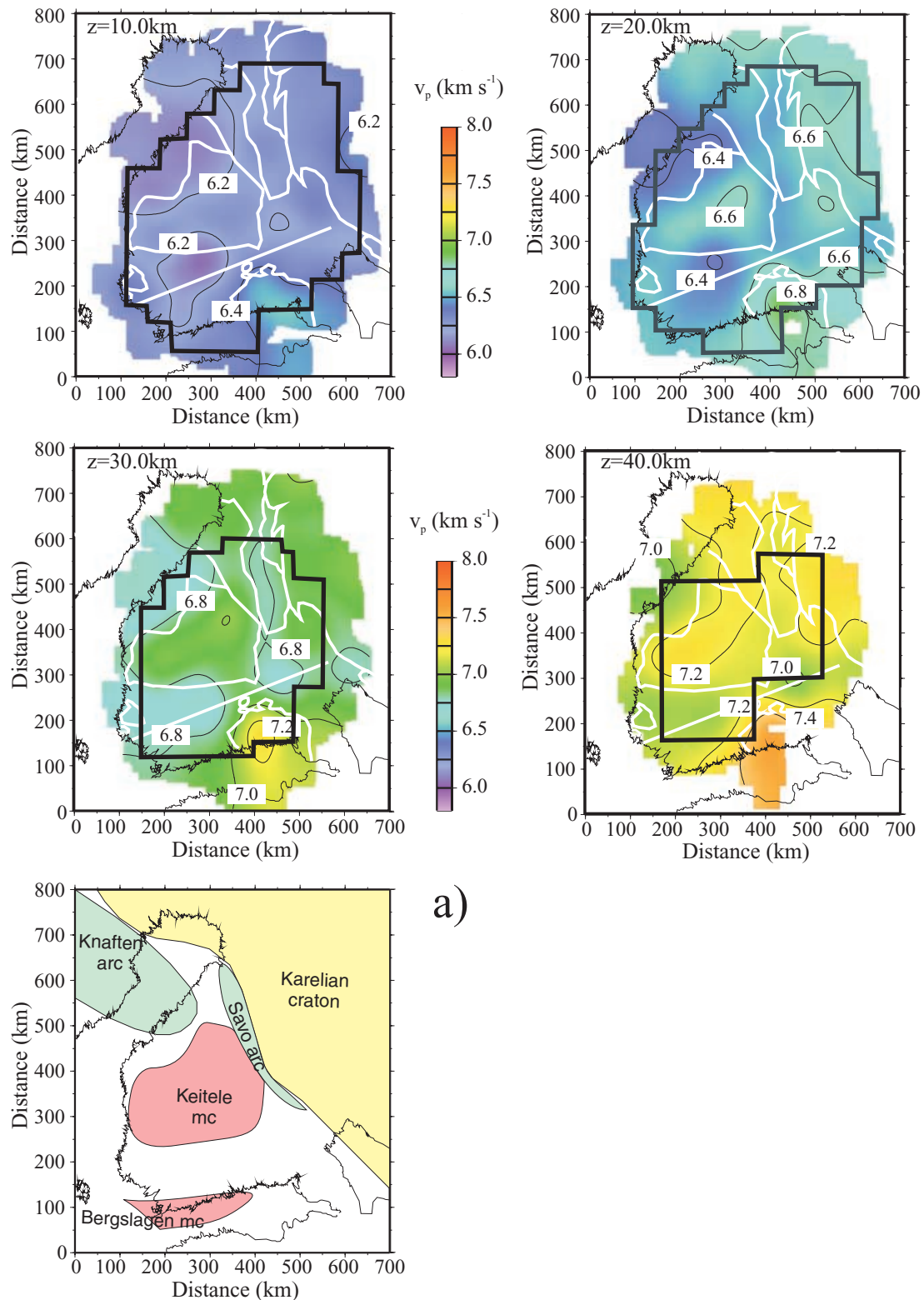
This effect is enhanced by the high velocities associated with the Mesoproterozoic rapakivi batholiths (VyR). Vertical  $V_p/V_s$  cross-sections display a structure with alternating minima and maxima; the minima are associated with schist belts (Bothnian Belt and Pirkanmaa Belt) and the maxima with the granitoid batholiths (Central Finland Granitoid Complex, Laitila Rapakivi granite and Vyborg Rapakivi granite).

## DISCUSSION

Our crustal velocity model combines both local seismic data and refraction seismic data sets. The absolute  $P$ - and  $S$ -wave velocities are inverted in a 3-D model grid with cell size of  $60 \times 60 \times 6 \text{ km}^3$  spanning a volume of  $700 \times 800 \times 70 \text{ km}^3$ . Absolute velocity models have several advantages over relative velocity models; the model

values can easily be compared with previous refraction study results, it gives an independent estimate of the 3-D  $V_p/V_s$  or Poisson's ratio ( $\sigma$ ) distribution in the crust, and the model can be used in locating seismic events more accurately.

The previously published crustal models in this area (Korja *et al.* 1993; Luosto 1997; Sandoval *et al.* 2003; Kozlovskaya *et al.* 2004) are mainly based on interpolation of available seismic refraction profile data. Our model is based on data gathered all over the study area, and the ray paths transect the study volume in all directions (e.g. Fig. 5). Thus, the tomography modelling gives a more comprehensive approximation of the 3-D velocity structures than obtained from interpolation of 2-D seismic refraction results. The wealth of new data enables to resolve the crustal structure more detailed, especially, in areas between the DSS survey lines, where previous crustal models assume velocity continuity (Korja *et al.* 1993; Luosto 1997; Sandoval *et al.* 2003).



a)

**Figure 6.** Lateral distribution of the  $P$ - and  $S$ -wave velocity and  $V_p/V_s$  models. (a)  $P$ -wave velocity distribution at depths of 10, 20, 30 and 40 km. (b)  $S$ -wave velocity distribution is shown at depths of 10, 20, 30 and 40 km. (c)  $V_p/V_s$  distribution is presented at depths of 10, 20, 30 and 40 km. The approximated Poisson's ratio is indicated in the  $V_p/V_s$ -scale bar. White lines delimit the main geological features according to Fig. 1. The Bergslagen and Keitele microcontinental (mc) fragments are outlined in the bottom map.

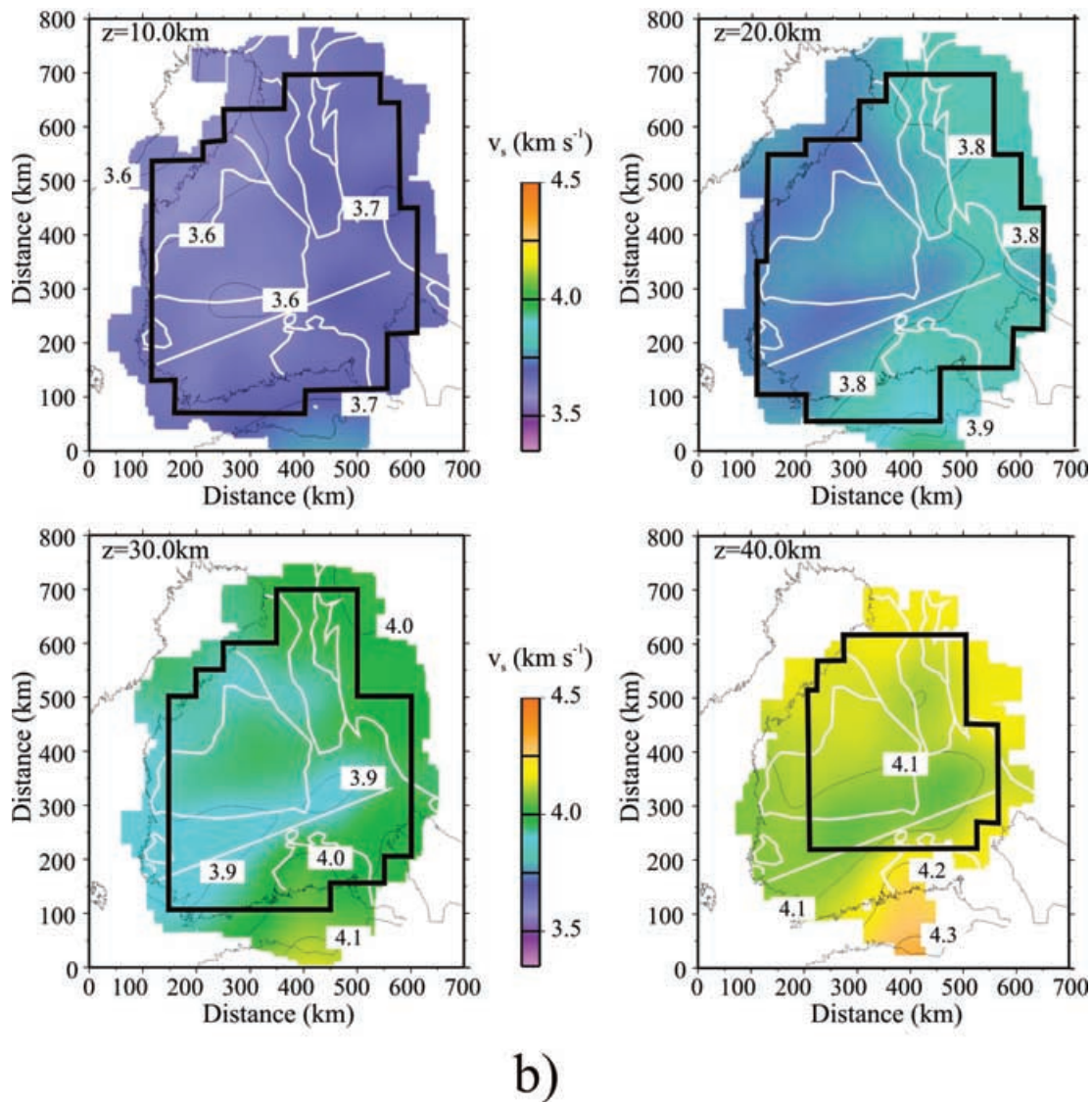


Figure 6. (Continued.)

In Fig. 8, the tomographic model is compared with the 2-D ray-traced model along the BALTIC profile. In general, these models show good agreement. In the 2-D ray-trace modelling (Grad & Luosto 1987; Luosto *et al.* 1990, 1995; Heikkinen *et al.* 1998) layer boundaries are introduced and a certain lateral continuity of the layers is required. Abrupt horizontal changes in material properties are difficult to image, and thus these models contain inherent lateral continuity. On the other hand, the introduction of layer boundaries increases the vertical resolution in the models as both reflected and refracted waves are used (Zelt *et al.* 2003). In tomographic models, the lack of layer boundaries results in smoothed vertical seismic velocity distribution. For example, the upper-crustal high-velocity bodies of the 2-D model of the BALTIC profile, beneath the Vyborg Rapakivi area (VyR) and the Outokumpu ophiolite formation (OB; Luosto *et al.* 1990) are replaced by upwarping of the isolines in the tomography model (Fig. 8). The lack of crustal boundaries may also increase average velocities in the lower part of the model, because a velocity gradient high enough is needed for rays to turn in the crust (Fig. 8).

The new 3-D crustal model suggests that the velocity distributions are laterally more variable than the previous models (Sandoval *et al.*

2003) image and that the crust is composed of alternating high- and low-velocity pieces or blocks. The lateral crustal block size varies between 100 and 200 km, which is approximately twice the spatial model resolution. Recently the BABEL reflection data set suggested similar crustal block sizes (Korja & Heikkinen 2005). It is inferred that interpolated models based on refraction lines with 100–200 km line spacing are likely to miss some of the crustal units and thus the crustal geometry is oversimplified.

Sandoval *et al.* (2003) calculated a new 3-D crustal  $P$ -wave velocity model in order to make crustal corrections to the SVEKALAPKO teleseismic  $P$ -wave tomography model of the mantle lithosphere. Their model is based on interpolating the pre-SVEKALAPKO controlled source data into a 3-D velocity matrix. However, the addition of the SVEKALAPKO local events has brought up a few differences of which an example is given by comparing Fig. 9 with Fig. 6(a) at depth of 20 km.

The major difference is a NE–SW directed anomaly in the middle and lower crust (20–40 km) beneath central Finland, which is a negative low-velocity anomaly ( $V_p < 6.4 \text{ km s}^{-1}$ ; at 20 km) in Sandoval *et al.* (2003) model (Fig. 9) and a positive, high-velocity anomaly ( $V_p = 6.4\text{--}6.6 \text{ km s}^{-1}$ ) in our model (Fig. 6a). The average velocity

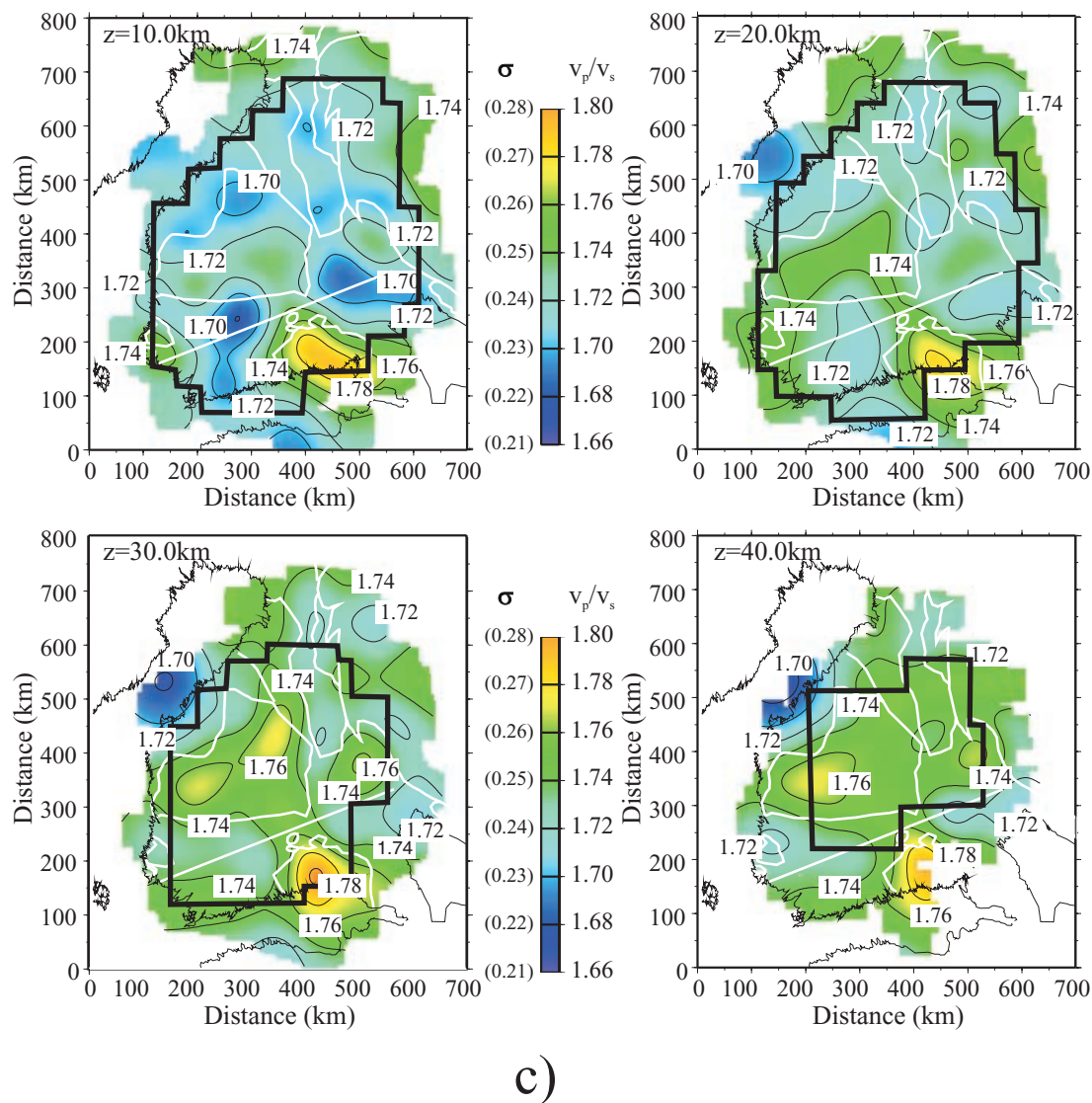
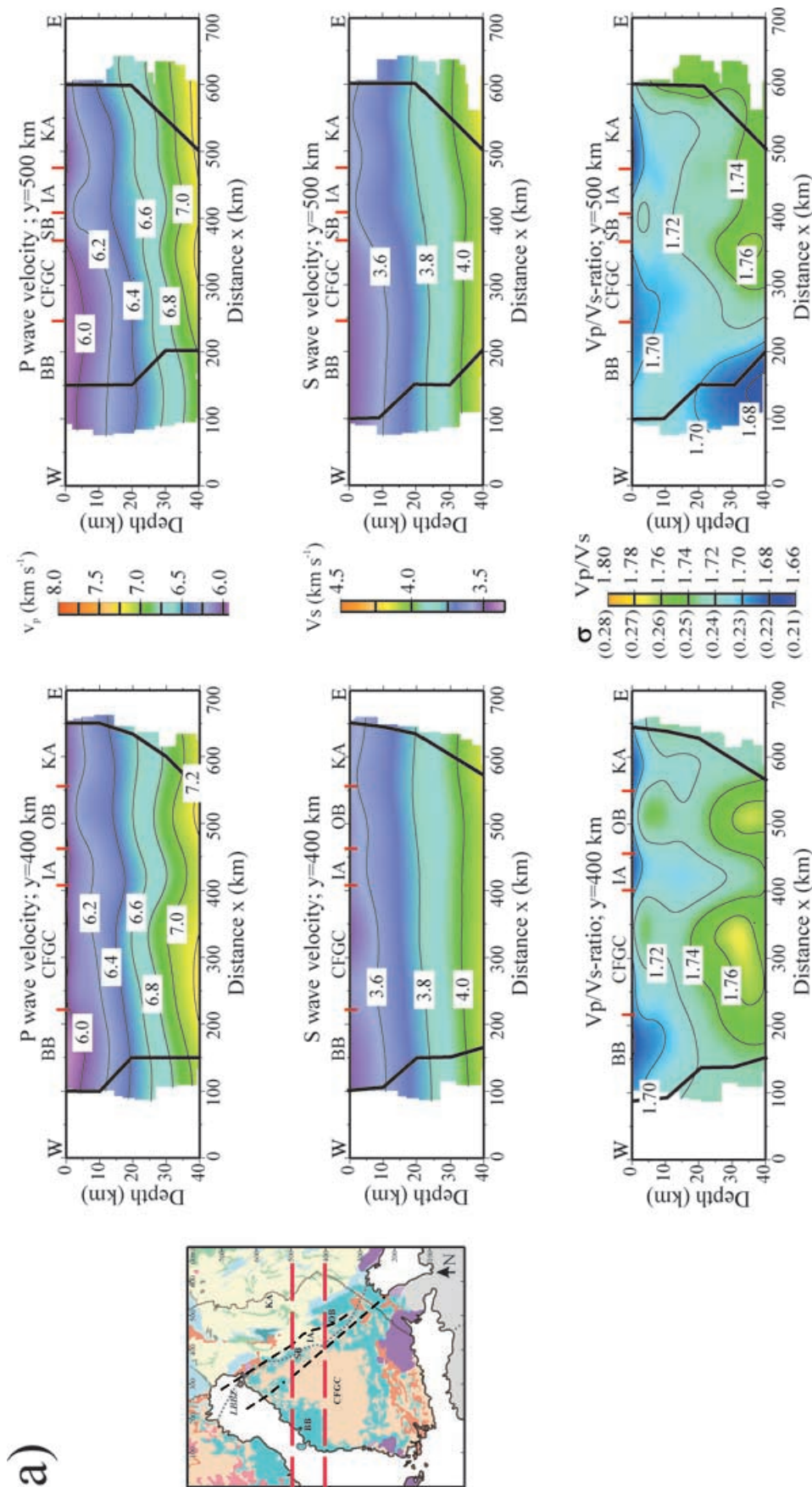


Figure 6. (Continued.)

difference is  $0.2\text{--}0.4\text{ km s}^{-1}$  and 3–4 per cent in depth column of 20–40 km. The same anomaly shape of Fig. 9 is repeated in the uppermost mantle with an opposite, positive sign (+2 per cent), at depth of 70 km, in the teleseismic upper-mantle model by Sandoval *et al.* (2004). Similar pattern is also present in a residual Bouguer anomaly map (Kozlovskaya *et al.* 2004) after removing the crustal effect of the Sandoval *et al.* (2003) model. We argue that this crustal high-velocity anomaly is real and is already outlined in the map showing the high-velocity layer in the lower crust by Korja *et al.* (1993). The same anomaly is detected as high velocities in the middle and lower crust ( $6.6\text{--}6.9\text{ km s}^{-1}$  between depths 20 and 40 km) in the SVEKALAPKO local tomography profiles by Yliniemi *et al.* (2004). The positive Bouguer anomaly associated with this anomaly (Kozlovskaya *et al.* 2004) indicates that the high-velocity anomaly is composed of material with positive density contrast. Because it is also associated with high  $V_p/V_s$  ratio  $>1.76$  (Fig. 6c) we interpret that the NE–SW anomaly is composed of mafic material and may record mafic under and intraplating of the crust as suggested by Korja *et al.* (1993). An implication of this interpretation is that the positive mantle anomaly would be diluted and that the velocity dif-

ference between Proterozoic and Archean mantle anomalies would be less pronounced. Another implication is that in structurally complex areas, such as the accretionary Svecofennian Orogen, crustal corrections for teleseismic data should be based on 3-D data sets if available.

An example of the correlation of the model with the surface geology is made in detail along the BALTIC profile (Fig. 8). The metasedimentary rocks (Southern Finland Belt and Outokumpu Belt) are associated with velocity minima and the granitoid rocks in the Vyborg rapakivi granite area (VyR) and in the Archean part (KA) with local maxima. The Archean part has the highest surface velocities. A high velocity upper-crustal body ( $V_p > 6.0\text{ km s}^{-1}$ ) embedded in the low velocity background ( $V_p < 5.6\text{ km s}^{-1}$ ) below the Outokumpu area, is interpreted to represent the Outokumpu ophiolite sequence interbedded with the metaturbidites (Luosto *et al.* 1990; Korja *et al.* 1993). Another high velocity body ( $V_p > 6.5\text{ km s}^{-1}$  at depth of 15 km) beneath the Vyborg rapakivi granite is interpreted as a mafic gabbro-anorthosite body belonging to the rapakivi bimodal magmatic association (Elo & Korja 1993; Haapala & Rämö 1999).



**Figure 7.** Vertical velocity cross-sections of the study area. (a)  $P$ - and  $S$ -wave velocity and  $V_p/V_s$  distribution along W-E oriented lines  $y = 400$  and  $500$  km across the study region. (b)  $P$ - and  $S$ -wave velocity and  $V_p/V_s$  distribution along S-N oriented lines  $x = 400$  and  $260$  km across the study region. The approximated Poisson's ratio is indicated in the  $V_p/V_s$ -scale bar. Black line marks out the region with satisfactory resolution. Abbreviations: BB, Bothnian Belt; CFGC, Central Finland Granitoid Complex; SB, Savo Belt; IA, Iisalmi Archean Terrane; OB, Outokumpu Belt; KA, Karelian Archean Terrane; LBBZ, Ladoga Bothnian Bay Zone; Vyb, Vyborg Rapakivi Batholiths; Pib, Pirkankmaa Belt; SFB, Southern Finland Belt.

Downloaded from <https://academic.oup.com/gji/article/168/3/1210/931281> by guest on 05 March 2021

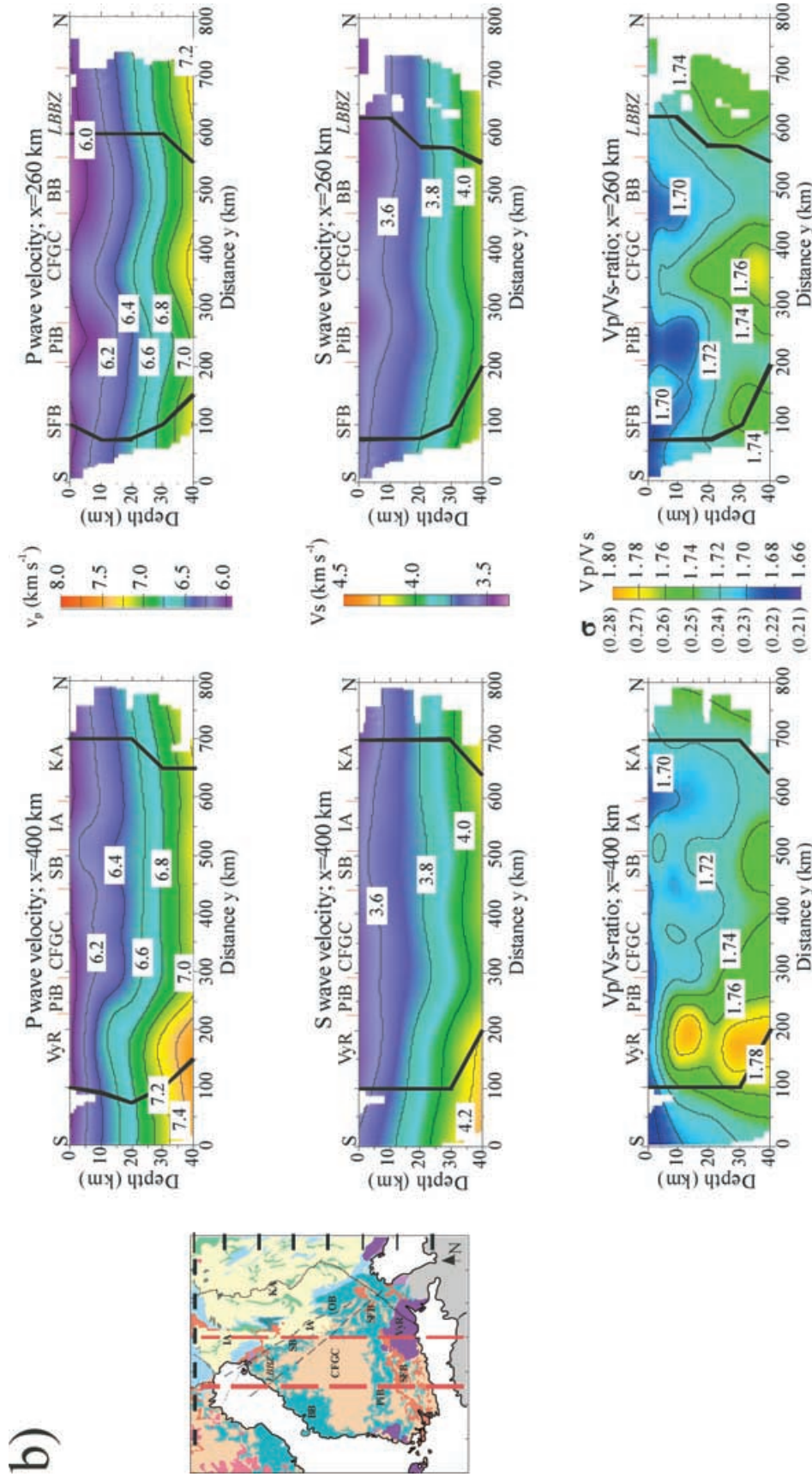
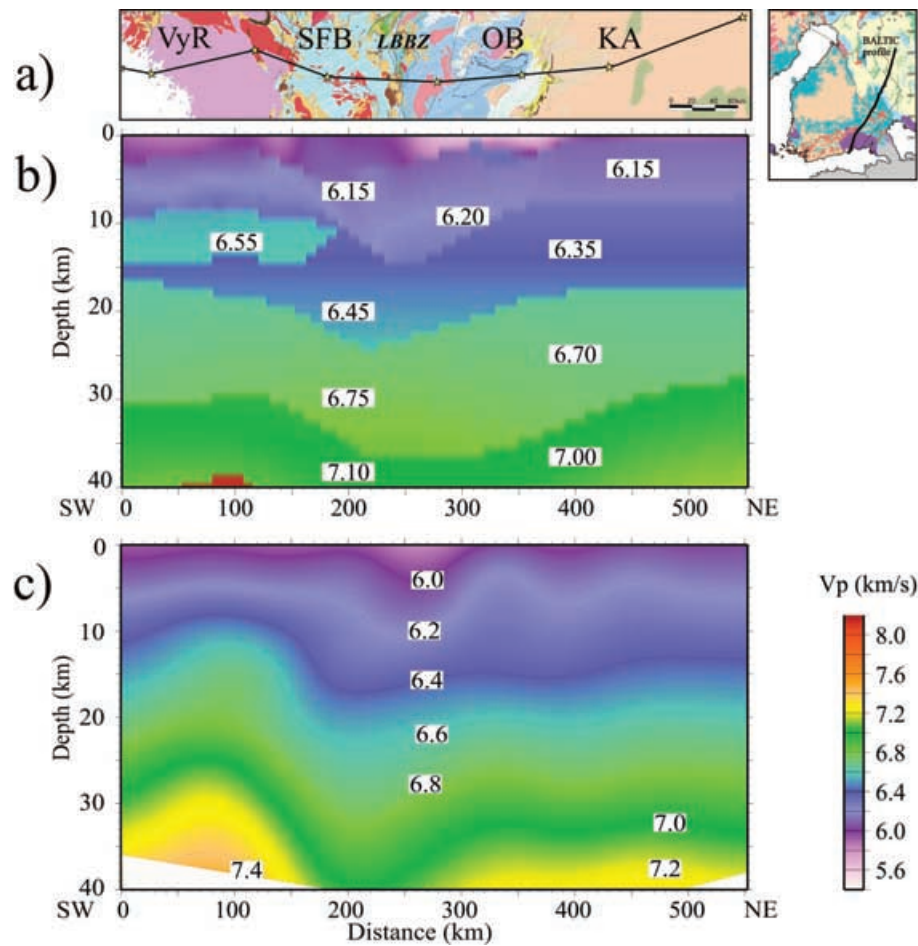


Figure 7. (Continued.)



**Figure 8.** Tomographic model versus ray-traced model of the BALTIC profile. The location of the profile is shown on an insert map. (a) Geological transect around the BALTIC profile after Korsman *et al.* (1997). Abbreviations: VyR, Vyborg Rapakivi Batholiths; SFB, Southern Finland Belt; LBBZ, Ladoga Bothnian Bay Zone; OB, Outokumpu Belt; KA, Karelian Archean Terrane. Legend: tan, Archean: tan, granite and gneiss; light green, greenstone; Palaeoproterozoic; yellow, meta-arenites; purple, ophiolite; blue, mica schist and gneiss; green, metavolcanic rocks; red, granitoids; brown, gabbroic rocks; lilac, rapakivi granite. (b) *P*-wave ray-traced model of the BALTIC profile after Luosto *et al.* (1990). (c) Tomographic *P*-wave velocity model is shown along the BALTIC profile.

In the study area, the lower and middle crust beneath granitoid complexes (VyR, CFGC, KA) is characterized by *ca.* 0.1 km s<sup>-1</sup> higher *P*-wave velocities, *ca.* 0.05 km s<sup>-1</sup> higher *S*-wave velocities, *ca.* 0.04 higher *V<sub>p</sub>/V<sub>s</sub>* ratios (Figs 6 and 7) and 2–3 per cent higher densities (Elo & Korja 1993; Kozlovskaya *et al.* 2004) than the surrounding areas. In the Vyborg rapakivi area, this is interpreted as mafic intra and underplating associated with the anorogenic A-type rapakivi granite formation (Elo & Korja 1993; Haapala & Rämö 1999). In central Finland, similar underplating process is invoked to explain the intrusion of post-kinematic, A-type granitoids (Elliott *et al.* 1998; Nironen *et al.* 2000). A similar type of positive velocity anomaly is found in the middle and lower crust beneath the Outokumpu Belt (Figs 6c and 7a) suggesting wider extends of the under and intraplating. We suggest that continuation of the tomographic model to the lowermost crust and detailed mapping of high *V<sub>p</sub>* and *V<sub>p</sub>/V<sub>s</sub>* ratio areas could provide an estimate of volume for mantle derived magmatism and its spatial distribution.

In the study area, the low *P*-wave velocity (*V<sub>p</sub>* < 6.0 km s<sup>-1</sup>) low *V<sub>p</sub>/V<sub>s</sub>* (<1.70) areas at surface and in the upper-crust correlate with schist belts (Figs 6 and 7). The vertical cross-sections (Fig. 7) show that these anomalies continue at depth, and the low-velocity metasedimentary material seems to dip under the high-velocity crustal blocks. In the western part of the study area, beneath

the Bothnian Belt (Figs 6c and 7a, *x* < 200 km, *y* = 450–600 km, *z* = 0–10 km and *z* = 20–40 km), a pronounced local velocity minimum (*V<sub>p</sub>* < 5.7 km s<sup>-1</sup> and *V<sub>p</sub>/V<sub>s</sub>* < 1.70) is associated with a low density (<3 · 10<sup>3</sup> km m<sup>-3</sup>) region modelled by Kozlovskaya *et al.* (2004). This upper-crustal velocity minimum is part of a larger minimum imaged in an inverted crustal model calculated from the BABEL wide-angle refraction data by Hole *et al.* (1996). The lower crustal anomaly coincides with the palaeo-accretionary prism found above a palaeosubduction zone (BABEL Working Group 1990; Korja & Heikkinen 2005). The geometrical distribution of seismic velocities is similar to modern environments where accretionary prisms are associated with lower velocities than the nearby arc crust (Suyehiro *et al.* 1996; Morozov *et al.* 2001; Shillington *et al.* 2004; Van Avendonk *et al.* 2004; Clowes *et al.* 2005). It is suggested that low seismic velocities *V<sub>p</sub>* < 5.7 km s<sup>-1</sup> together with low *V<sub>p</sub>/V<sub>s</sub>* ratios <1.7 carry a memory of the palaeo-accretionary prism environment. This implies that the lower velocity and lower *V<sub>p</sub>/V<sub>s</sub>* ratio is inherent material property of the layered, metasedimentary material which is not destroyed in metamorphic processes. In Lithoprobe SNORCLE transect, similar low *V<sub>p</sub>/V<sub>s</sub>* ratios <1.69 are imaged in the Palaeoproterozoic Hottah terrane, where they form a wide, shallowly dipping crustal terrane comprising quartz rich metasedimentary rocks (Fernández-Viejo *et al.* 2005).

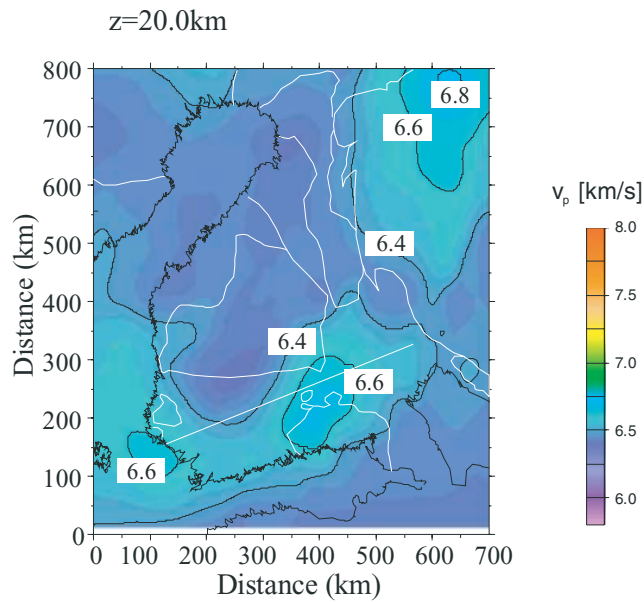


**Figure 9.**  $P$ -wave velocity model at depth of 20 km plotted from the velocity matrix of Sandoval *et al.* (2003) model (courtesy of Senen Sandoval). Corresponding depth slice of our model is shown in Fig. 6(a),  $z = 20$  km.

If it was true that the metasedimentary rocks carry *ca.*  $0.2 \text{ km s}^{-1}$  lower velocities and *ca.*  $0.04$  lower  $V_p/V_s$  ratios than magmatic rocks (Fig. 7) then the lateral variation of velocity minima and maxima could be interpreted to display the distribution of crustal slices and sedimentary basins within Central and Southern Finland. Based on geological and geophysical results Lahtinen *et al.* (2005) suggested that in addition to the outcropping arcs and sedimentary basins the Svecofennian Domain hosts also hidden microcontinents (e.g. Keitele and Bergslagen mc in Fig. 6). As the  $V_p$  and the  $V_p/V_s$  ratio anomaly patterns are similar to the proposed terrane distribution they not only support the idea of hidden microcontinents but they can be used to better outline them at depth. The minima correlate with the sedimentary basins and accretionary prisms and maxima with microcontinents and island arcs. This simplistic interpretation is complicated by post-collisional magmatic intra and underplating that has modified the lower crust as discussed above. Overall, the tomographic model supports the idea that the thick Svecofennian crust was accreted from several terranes and that the crust was later modified by intra and underplating.

## CONCLUSIONS

We have presented the first 3-D absolute velocity models where both  $P$ - and  $S$ -wave models have been inverted independently. It has several advantages over relative velocity models; the model values can easily be compared with previous refraction study results, it gives an independent estimate of the 3-D  $V_p/V_s$  or Poisson's ratio ( $\sigma$ ) distribution in the crust, and the model can be used in locating seismic events more accurately.

In structurally complex areas such as accretionary orogens, crustal corrections for teleseismic data should be based on 3-D data sets as interpolation of 2-D models may lead to oversimplification of the crustal structure.

Local seismic tomography method involving both  $P$ - and  $S$ -wave velocity and especially  $V_p/V_s$  ratio models can be used to map the spatial relationships of geological units in regional scale. Schist belts

and their continuations at depth are associated with lower velocities and lower  $V_p/V_s$  ratios ( $V_p < 6.2\text{--}6.8 \text{ km s}^{-1}$ ;  $V_s < 3.6\text{--}3.9 \text{ km s}^{-1}$ ;  $V_p/V_s = 1.68\text{--}1.73$ ) than the granitoid areas ( $V_p = 6.3\text{--}7.4 \text{ km s}^{-1}$ ;  $V_s = 3.6\text{--}4.2 \text{ km s}^{-1}$ ;  $V_p/V_s = 1.72\text{--}1.78$ ).

The Svecofennian Orogen was accreted from crustal blocks ranging in size between  $100 \times 100 \text{ km}^2$  and  $200 \times 200 \text{ km}^2$ . The crustal blocks have *ca.*  $0.2 \text{ km s}^{-1}$  higher velocity and *ca.*  $0.04$  higher  $V_p/V_s$  ratio than the intervening sedimentary belts or accretionary prisms. It is interpreted that the tomographic model images the hidden Keitele and Bergslagen microcontinents beneath the Central Finland Granitoid Complex and Southern Finland Belt, respectively. It is concluded that the tomographic model supports the idea that the thick Svecofennian crust was accreted from several terranes and that the crust was later modified by intra and underplating.

## ACKNOWLEDGMENTS

We would like to thank Dr Senen Sandoval for kindly providing us his 3-D crustal  $P$ -wave velocity model of the study area and Ms. Kati Karkkulainen for drafting the geological transects. We are greatly indebted to all participants, who successfully accomplished the EUROPROBE/SVEKALAPKO Seismic Tomography experiment. The SVEKALAPKO project was funded by the Academy of Finland and supported by the national science institutions in France, Germany, Poland, Russia, Sweden, Switzerland, the Czech Republic and the Netherlands. Finally, we would like to thank Peter Maguire and Thomas Funck for their thorough constructive reviews that substantially improved the manuscript.

The SVEKALAPKO Seismic Tomography Working Group members are U. Achauer, A. Alinaghi, J. Ansorge, G. Bock, M. Brunet, W. Friederich, M. Grad, A. Guterch, P. Heikkinen, S.-E. Hjelt, T. Hyvönen, J.-P. Ikonen, E. Kissling, K. Komminaho, A. Korja, E. Kozlovskaya, M. V. Nevsky, N. I. Pavlenkova, H. Pedersen, J. Plomerová, T. Raita, O. Yu. Riznichenko, R. G. Roberts, S. Sandoval, I. A. Sanina, N. V. Sharov, Z. H. Shomali, J. Tiikkainen, E. Wielandt, K. Wylegalla, J. Yliniemi, and Y. G. Yurov.

## REFERENCES

- Alinaghi, A., Kind, R., Hanka, W., Wylegalla, K., the TOR Working Group & the SVEKALAPKO Seismic Tomography Working Group, 2003. Receiver function analysis of the crust and upper mantle from the North German Basin to the Archean Baltic Shield, *Geophys. J. Int.*, **155**, 641–652.
- BABEL Working Group, 1990. Evidence for early Proterozoic plate tectonics from seismic reflection profiles in the Baltic Shield. *Nature*, **348**, 34–38.
- BABEL Working Group, 1993. Integrated seismic studies of the Baltic Shield using data in the Gulf of Bothnia region, *Geophys. J. Int.*, **112**, 305–324.
- Bassin, C., Laske, G. & Masters, G., 2000. The Current Limits of Resolution for Surface Wave Tomography in North America, *EOS, Trans. Am. geophys. Un.*, **81**, F897.
- Bock, G. & the SVEKALAPKO Seismic Tomography Working Group, 2001. Seismic probing of Archean and Proterozoic lithosphere in Fennoscandia, *EOS, Trans. Am. geophys. Un.*, **82**, 621, 628–629.
- Brunet, M., Farra, V., Pedersen, H.A. & the SVEKALAPKO Seismic Tomography Working Group, 2002. Non-linear surface wave phase velocity inversion based on ray theory, *Geophys. J. Int.*, **151**, 583–596.
- Brunet, M., Pedersen, H.A., Vacher, P., Kukkonen, I.T., Arndt, N.T., Funke, S., Friederich, W., et al., 2004a. Layered lithospheric mantle in the central Baltic Shield from surface waves and xenoliths analysis, *Earth planet. Sci. Lett.*, **226**, 41–52.

- Bruneton, M., Pedersen, H.A., Farra, V., Arndt, N.T., Vacher, P. & the SVEKALAPKO Seismic Tomography Working Group, 2004b. Complex lithospheric structure under the central Baltic Shield from surface wave tomography, *J. geophys. Res.*, **109**, B10303, doi: 10.1029/2003JB002947.
- Burmakov, Yu.A., Kosminskaya, I.A., Sharov, N.V., Korhonen, H., Luosto, U. & Yliniemi, J., 1991. Tomographic study of crustal velocity structure in southern Finland, *Tectonophysics*, **189**, 29–35.
- Clowes, R.M., Hammer, P.T., Fernández-Viejo, G. & Welford, J.K., 2005. Lithospheric structure in northwestern Canada from Lithoprobe seismic refraction and related studies: a synthesis, *Can. J. earth Sci.*, **42**, 1277–1293.
- Elliott, B.A., Rämö, O.T. & Nironen, M., 1998. Mineral chemistry constraints on the evolution of the 1.88–1.87 Ga post-kinematic granite plutons in the Central Finland Granitoid Complex, *Lithos*, **45**, 109–129.
- Elo, S. & Korja, A., 1993. Geophysical interpretation of the crustal and upper mantle structure in the Wiborg rapakivi gravity area, southeastern Finland, *Precambrian Res.*, **64**, 273–288.
- Farra, V., 1990. Amplitude computation in heterogeneous media by ray perturbation theory: a finite element approach, *Geophys. J. Int.*, **103**, 341–354.
- Fernández-Viejo, G., Clowes, R.M. & Welford, J.K., 2005. Constraints on the composition of the crust and uppermost mantle in northwestern Canada:  $V_p/V_s$  variations along Lithoprobe's SNorCLE transect, *Can. J. earth Sci.*, **42**, 1205–1222.
- Friederich, W., Funke, S. & the SVEKALAPKO Seismic Tomography Working Group, 2004. The resolution power of teleseismic surface wave tomography exemplified by the SVEKALAPKO array, *Geophys. Res. Abstracts*, **6**, 05811, European Geosciences Union 2004.
- Grad, M. & Luosto, U., 1987. Seismic models of the crust of the Baltic shield along the SVEKA Profile in Finland, *Ann. Geophys.*, **5B**(6), 639–650.
- Haapala, I. & Rämö, T., 1999. Rapakivi Granites and Related Rocks: an introduction, *Precambrian Res.*, **95**, 1–7.
- Hjelt, S.-E., Daly, S. & SVEKALAPKO colleagues, 1996. SVEKALAPKO Evolution of Palaeoproterozoic and Archean Lithosphere, in *EURO-PROBE 1996—Lithosphere Dynamics: Origin and Evolution of Continents*, pp. 56–67, eds Gee, D. & Zeyen, H., EUROPROBE Secretariat, Uppsala University.
- Heikkinen, P. & the FENNIA Working Group, 1998. *P* and *S* wave velocity structure of the Fennoscandian Shield beneath the FENNIA profile in southern Finland, *Inst. Seismology, Univ. Helsinki, Rep.* **S-38**, 14 pp.
- Henson, I. & Coyne, J.M., 1995. *Geotool Sourcebook: Users Manual*, 174 pp., Teledyne Brown Engineering, Huntsville.
- Hobro, J.W.D., 1999. Three-dimensional tomographic inversion of combined reflection and refraction seismic travel-time data, *PhD thesis*, Department of Earth Sciences, University of Cambridge, Cambridge, 299 pp.
- Hobro, J.W.D., Singh, S.C. & Minshull, T.A., 2003. Three-dimensional tomographic inversion of combined reflection and refraction seismic traveltimes data, *Geophys. J. Int.*, **152**, 79–93.
- Hole, J.A., Fliedner, M.M. & Klempner, S.L., 1996. Three-dimensional analysis and inversion of BABEL seismic refraction data from the Bothnian Sea, in *The BABEL project—Final status report, Deep Reservoir Geology Programme, EUR 16486*, pp. 135–141, eds Meissner, R., Blundell, D., Snyder, D. & McBride, J., European Commission, Luxembourg.
- Hyvönen, T. & Sanina, I.A., 1996. Statistical search for inhomogeneities of the lithosphere in central Finland, in *Seismology in Europe, Papers presented at the XXV General Assembly of European Seismological Commission*, 9–14 September 1996, Reykjavik, Iceland, pp. 214–119.
- Kinck, J., Husebye, E.S. & Larsson, F., 1993. The Moho depth distribution in Fennoscandia and the regional tectonic evolution from Archean to Permian times, *Precambrian Res.*, **64**(1–4), 23–51.
- Koistinen, T., Stephens, M.B., Bogatchev, V., Nordgulen, U., Wennerström, M., Korhonen, J. (Eds.), 2001. *Geological map of the Fennoscandian Shield, scale 1:2 000 000*, Geological Survey of Finland, Geological Survey of Norway, Geological Survey of Sweden, Ministry of Natural Resources of Russia, Espoo, Trondheim, Uppsala, Moscow.
- Korja, A. & Heikkinen, P., 2005. The accretionary Svecofennian orogen—insight from the BABEL profiles, *Precambrian Res.*, **136**, 241–268.
- Korja, A., Korja, T., Luosto, U. & Heikkinen, P., 1993. Seismic and geoelectric evidence for collisional and extensional events in the Fennoscandian Shield—implications for Precambrian crustal evolution, *Tectonophysics*, **219**, 129–152.
- Korsman, K., Koistinen, T., Kohonen, J., Wennervirta, M., Ekdahl, E., Honkamo, M., Idman, H. & Pekkala, Y. (Eds.), 1997. Bedrock map of Finland 1:1 000 000. *Geol. Survey Finland*, Espoo.
- Korsman, K., Korja, T., Pajunen, M., Virransalo, P. & GGT/SVEKA Working Group, 1999. The GGT/SVEKA Transect—Structure and evolution of the continental crust in the Paleoproterozoic Svecofennian Orogen in Finland, *Int. Geol. Rev.*, **41**, 287–333.
- Kozlovskaya, E., Elo, S., Hjelt, S.E., Yliniemi, J., Pirttijärvi, M. & the SVEKALAPKO Seismic Tomography Working Group, 2004. 3-D density structure of the crust of southern and central Finland obtained from joint interpretation of the SVEKALAPKO crustal *P* wave velocity models and gravity data, *Geophys. J. Int.*, **158**, 827–848.
- Lahtinen, R., Korja, A. & Nironen, M., 2005. Paleoproterozoic tectonic evolution, in eds Lehtinen, M., Nurmi, P.A. & Rämö, O.T., (red.): *Precambrian Geology of Finland—Key to the Evolution of the Fennoscandian Shield*, Elsevier Science, B.V., Amsterdam, pp. 481–532.
- Luosto, U., 1991. Crustal structures of eastern Fennoscandia, *Tectonophysics*, **189**, 19–27.
- Luosto, U., 1997. Structure of the Earth's Crust in Fennoscandia as Revealed from refraction and Wide-Angle Reflection Studies, *Geophysica*, **33**(1), 3–16.
- Luosto, U., Flüh, E.R., Lund, C.-E. & Working Group, 1989. The crustal structure along the POLAR profile from seismic reflection investigations, *Tectonophysics*, **162** 51–85.
- Luosto, U. *et al.*, 1990. Crust and upper mantle structure along the DSS Baltic profile in SE Finland, *Geophys. J. Int.*, **101**, 89–110.
- Luosto, U. *et al.*, 1995. Crustal structure along the Sveka'91 profile in Finland, in *Proc. and Activity Rep. 1992–1994 Vol. II, ESC XXIV General Assembly, 1994 September 19–24 Athens, Greece*, pp. 974–983, eds Makropoulos, K. & Suhadolc, P., Univ. Athens, Athens.
- McCaughy, M. & Singh, S., 1997. Simultaneous velocity and interface tomography of normal-incidence and wide-aperture seismic traveltimes data, *Geophys. J. Int.* **131**, 87–99.
- Malaska, J. & Hyvönen, T., 2000. Velocity modelling of the lithosphere beneath South Finland, *Phys. Earth planet. Int.*, **122**(1–2), 103–114.
- Mooney, W.D., Laske, G. & Masters, G.T., 1998. CRUST 5.1; a global crustal model at 5 degrees × 5 degrees, *J. geophys. Res.*, **103**, 727–747.
- Morozov, I.B., Smithson, S.B., Chen, J. & Hollister, L.S., 2001. Generation of new continental crust and terrane accretion in southeastern Alaska and western British Columbia: constraints from *P*- and *S*-wave wide-angle data (ACCURETE), *Tectonophysics*, **341**, 49–67.
- Nironen, M., Elliott, B.A. & Rämö, O.T., 2000. 1.88–1.87 Ga post-kinematic intrusions of the Central Finland Granitoid Complex: a shift from C-type to A-type magmatism during lithospheric convergence, *Lithos*, **53**, 37–58.
- Ollikainen, M. & Ollikainen, M. (Eds.), 2004. *The Finnish Coordinate Reference Systems*, Finnish Geodetic Institute and National Land Survey, p. 18, <http://www.maanmittauslaitos.fi/default.asp?id=0&docid=2507>.
- Press, W.H., Teukolsky, S.A., Vetterling, W.T. & Flannery, B.P., 1992. *Numerical Recipes in FORTRAN: The Art of Scientific Computing*, 2nd edn, Cambridge University Press, New York.
- Poupinet, G., Mäntyniemi, P., Luosto, U. & Achauer, U., 1993. A teleseismic study of the lithospheric structure along the Ladoga-Bothnian Bay zone in Finland, *Tectonophysics*, **219**, 153–161.
- Raita, T., 2001. The seismic tomography experiment of the SVEKALAPKO project. *M.Sc. thesis*. Dept. of Geophysics, Oulu University, 96 pp.
- Sandoval, S., Kissling, E., Ansorge, J. & the SVEKALAPKO Seismic Tomography Working Group, 2003. High-resolution body wave tomography beneath the SVEKALAPKO array: I. A priori three-dimensional crustal model and associated traveltimes effects on teleseismic wave fronts, *Geophys. J. Int.*, **153**, 75–87.
- Sandoval, S., Kissling, E., Ansorge, J. & the SVEKALAPKO Seismic Tomography Working Group, 2004. High-resolution body wave tomography beneath the SVEKALAPKO array: II. Anomalous upper mantle structure beneath the central Baltic Shield, *Geophys. J. Int.*, **157**, 200–214.
- Shillington, D.J., Van Avendonk, H., Holbrook, W.S., Kelemen, P. & Hornbach, M., 2004. Composition and structure of the central Aleutian

- island arc from arc-parallel wide-angle seismic data, *Geochem. Geophys. Geosyst.*, **5**, Q10006, doi:10.1029/2004GC000715.
- Šroda, P., 1999. Modifications of software package ZPLOT by C. Zelt, *Inst. Geophys. Pol. Acad. Sc.*, Warsaw.
- Suyehiro, K. *et al.*, 1996. Continental crust, crustal underplating, and low-Q upper mantle beneath an oceanic island arc, *Science*, **272**, 390–392.
- Tong, C.H., 2002. Model parameterisation and assessment in travelttime seismic tomography: a user's perspective, *Lithos Science Rep. March 2000*, **2**, 101–107.
- Van Avendonk, H.J.A., Shillington, D.J., Holbrook, W.S. & Hornbach, M.J., 2004. Inferring crustal structure in the Aleutian island arc from a sparse wide-angle seismic data set, *Geochem. Geophys. Geosyst.*, **5**, Q08008, doi:10.1029/2003GC000664.
- Wessel, P. & Smith, W.H.F., 1998. New improved version of the Generic Mapping Tools Released, *EOS, Trans. Am. geophys. Un.*, **79**, 579.
- Williamsson, P.R., 1990. Tomographic inversion in reflection seismology. *Geophys. J. Int.*, **100**, 255–274.
- Yliniemi, J., Kozlovskaya, E., Hjelt, S.E., Komminaho, K., Ushanov, A. & the SVEKALAPKO Seismic Tomography Working Group, 2004. Structure of the crust and uppermost mantle beneath southern Finland revealed by analysis of local events registered by the SVEKALAPKO seismic array, *Tectonophysics*, **394**(1–2), 41–67.
- Zelt, C.A., 1994. *ZPLOT—An interactive plotting and picking program for seismic data*, Bullard Lab., Univ. of Cambridge, Cambridge, UK.
- Zelt, C.A., 1998. Lateral velocity resolution from three-dimensional seismic refraction data, *Geophys. J. Int.*, **135**, 1101–1112.
- Zelt, C.A., Sain, K., Naumenko, J.V. & Sawyer, D.S., 2003. Assessment of crustal velocity models using seismic refraction and reflection tomography, *Geophys. J. Int.*, **153**, 609–626.